4-3-2020

Covalent Complex of DNA and Bacterial Topoisomerase: Implications in Antibacterial Drug Development

Purushottam B. Tiwari
Department of Oncology, Georgetown University

Prem P. Chapagain
Department of Physics, Florida International University, chapagap@fiu.edu

Ahmed Seddek
Biomolecular sciences institute, Florida International University

Thirunavukkarasu Annamalai
Biomolecular sciences institute, Florida International University, Miami, FL 33199, USA., athiruna@fiu.edu

Aykut Üren
Department of Oncology, Georgetown University

See next page for additional authors

Recommended Citation

Tiwari PB, Chapagain PP, Seddek A, Annamalai T, Üren A, Tse-Dinh YC. Covalent Complex of DNA and Bacterial Topoisomerase: Implications in Antibacterial Drug Development. ChemMedChem. 2020 Apr 3;15(7):623-631. doi: 10.1002/cmdc.201900721. Epub 2020 Mar 18. Erratum in: ChemMedChem. 2021 Jun 18;: PMID: 32043806; PMCID: PMC7133791.

HHS Public Access

Author manuscript

ChemMedChem. Author manuscript; available in PMC 2021 April 03.

Published in final edited form as:

ChemMedChem. 2020 April 03; 15(7): 623–631. doi:10.1002/cmdc.201900721.

Covalent Complex of DNA and Bacterial Topoisomerase: Implications in Antibacterial Drug Development

Purushottam B. Tiwari[a], **Prem P. Chapagain**[b],[c], **Ahmed Seddek**[c],[d], **Thirunavukkarasu Annamalai**[c],[d], **Aykut Üren**[a], **Yuk-Ching Tse-Dinh**[c],[d]

[a]Department of Oncology, Georgetown University, Washington, DC 20057 (USA)

[b]Department of Physics, Florida International University, Miami, FL 33199 (USA)

[c]Biomolecular sciences institute, Florida International University, Miami, FL 33199 (USA)

[d]Department of Chemistry and Biochemistry, Florida International University, Miami, FL 33199 (USA)

Abstract

A topoisomerase-DNA transient covalent complex can be a druggable target for novel topoisomerase poison inhibitors that represent a new class of antibacterial or anticancer drugs. Herein, we have investigated molecular features of the functionally important *Escherichia coli* topoisomerase I (EctopoI)-DNA covalent complex (EctopoIcc) for molecular simulations, which is very useful in the development of new antibacterial drugs. To demonstrate the usefulness of our approach, we used a model small molecule (SM), NSC76027, obtained from virtual screening. We examined the direct binding of NSC76027 to EctopoI as well as inhibition of EctopoI relaxation activity of this SM via experimental techniques. We then performed molecular dynamics (MD) simulations to investigate the dynamics and stability of EctopoIcc and EctopoI-NSC76027-DNA ternary complex. Our simulation results show that NSC76027 forms a stable ternary complex with EctopoIcc. EctopoI investigated here also serves as a model system for investigating a complex of topoisomerase and DNA in which DNA is covalently attached to the protein.

Graphical Abstract

P. B. Tiwari, pbt7@georgetown.edu.

Conflict of interest

The authors declare no conflict of interest.

Supporting information and the ORCID identification number(s) for the author(s) of this article can be found under: https://doi.org/10.1002/cmdc.201900721.

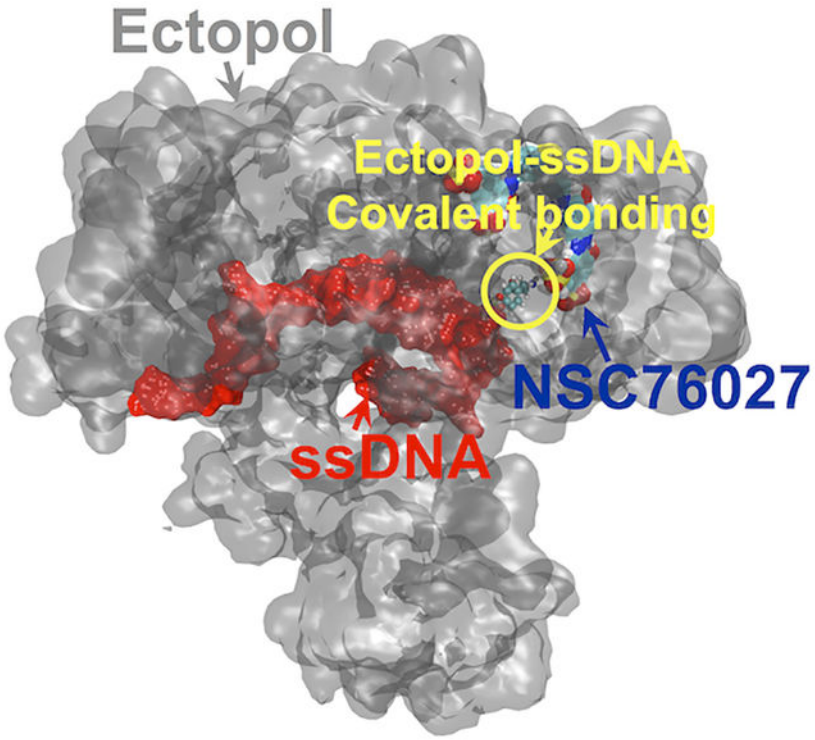

This report presents an approach to design functionally important covalent complex between bacterial topoisomerase and DNA for molecular simulations, which is very useful in development of new antibacterial drugs. Our results demonstrate the suitability of the model and procedures employed in this report for computational studies of inhibitors targeting topoisomerases.

Keywords

Antibacterial drugs; MD simulation; Surface plasmon resonance; Topoisomerase-DNA covalent complex; Topoisomerase inhibitors

Introduction

DNA topoisomerases are responsible for regulation of DNA topology, a crucial cellular process, which is very important in replication, transcription and recombination.[1] Topoisomerase I (topoI) cleaves and rejoins the single strand of DNA with a transient covalent complex.[2] These covalent complexes can be trapped by topoisomerase poison inhibitors.[3] Development of topoisomerase poison inhibitors have clinical applications as antitumor[4] antiviral[5] and antibacterial drugs.[6]

Previous genetic studies showed that the accumulation of the topoI-DNA covalent cleavage complexes (topoccs) in *Escherichia coli* can cause the bacterial cell death.[7] Bacterial DNA topoI belonging to the type IA topoisomerase family maintains the genome stability[8] and is a promising target biomolecule for antibacterial drug discovery[7a, 9] with *E. coli* topoisomerase I (EctopoI) as the most extensively studied member of the type IA

topoisomerase family.[10] In EctopoI, Y319 is the active site tyrosine, which is responsible for the formation of transient covalent linkage with the 5' phosphoryl group of cleaved DNA.[11] In *E. coli*, EctopoI regulates the DNA supercoiling by removing excess negative supercoils.[12] In recent years, bacterial pathogens have become more resistant to available antibacterial drugs, thus becoming a serious public health issue. There is at least one type IA topoI in each bacterium and a new class of poison inhibitors can be utilized to target these topoisomerases.[7a] It is therefore highly desirable to identify the poison inhibitors for type IA topoI for the development of new antibacterial drugs.[3, 7a, 9a] Development of such new antibacterial drugs requires investigations of topoIccs.

Computational approaches have proved to be very useful in structure based drug discovery, including hit identification and lead optimization[13] as well as in investigating drug specificity.[14] These computation-based approaches include docking[15] virtual screening (VS)[16] and molecular dynamics (MD) simulations.[17] Despite development of many docking algorithms, the results from these algorithms have limitations in the success of binding predictions.[18] Computer-aided virtual screening can be used to predict ligand binding to a receptor[19] but it has limitations in incorporating receptor flexibility.[20] Binding of a drug molecule to its target, more importantly protein, is a dynamic process[17a] and proteins are flexible biomolecules with a relatively small number of atoms in an average residue.[21] The dynamic flexibility of protein biomolecules can be incorporated via all-atom MD simulation[22], which is beneficial to explore drug targets.[23] Therefore, complementing the docking or VS results with MD simulations can be an effective strategy in the structure-based drug discovery.[18] However, MD simulations-aided investigations for structure-based drug discovery of antibacterial drugs involving bacterial topoIccs are lacking. This is mostly due to the difficulty in using the functionally important intermediate topoI structure in molecular simulations because the intermediate structure consists of a DNA fragment that is covalently complexed with the protein. In the past, MD simulation-based investigations of human topoisomerases (Htopos) in covalent complex with DNA (Htopocc) have been carried out.[24] Nevertheless, the simulation parameters are not provided for straightforward application without any optimizations and with no clear evidence of the covalent complex formation. Here, we used available CGenFF force field parameters to create linkage of EctopoI with the DNA single strand, providing an easy option with more straightforward procedure, so that MD simulations can be carried out for the EctopoI in covalent complex with DNA that has 5' phosphodiester bond with tyrosine. Our procedure provides an easy and straightforward option to create the DNA-protein covalent linkage for computational investigations using CHARMM36m force field for MD simulation-based investigations of the bacterial topoIccs with implications in antibacterial drug discovery, for the first time to the best of our knowledge.

To demonstrate the usefulness of our approach in the new antibacterial drug development, we used a model SM, NSC76027, obtained from a virtual screening (VS) of NCI DTP library of small molecules (SMs). We used a minimized the covalent complex of EctopoI with a single stranded DNA (ssDNA), referred to as EctopoIcc hereafter, as well as EctopoI conformation, taken from the same EctopoIcc, as the screening targets. Our virtual screening approach with both EctopoIcc and EctopoI alone will avoid toxic topoI inhibitors that bind non-selectively to DNA. We examined the direct binding of NSC76027 to EctopoI as well

inhibition of EctopoI relaxation activity of this SM utilizing experimental techniques. Surface plasmon resonance (SPR)-based experiments were performed to validate the direct binding of NSC76027 to EctopoI. In vitro relaxation inhibition assay for NSC76027 confirmed its inhibition of EctopoI activity. We then performed MD simulations to investigate the dynamics of the EctopoI-NSC76027-DNA complex (referred to as ternary complex hereafter). In the ternary structure, we constructed a covalent bond between EctopoI and a ssDNA using our procedure. Our approach is also useful in the MD simulation-based studies of other type of topoccs, including HtopoI, a major target biomolecule of anticancer agents.[25]

Results

EctopoI-DNA covalent complex and energy minimization

Figure 1 shows the covalent linkage of EctopoI with ssDNA from the minimized structure of EctopoIcc. The dotted circle in the Figure 1 shows the phosphorylated EctopoI Y319 with one of the side chain oxygen atoms (O^{S}_{319}) covalently linked with 5’ DNA carbon of thymine in the 9th position ($C^{5'}_{9}$). This model serves as the covalent complex between DNA nucleotide and Y319. Our procedure is able to handle such a covalent linkage between bacterial topoI and DNA and therefore can be used to explore interactions of this important protein-DNA interaction. A topology file (TYDN.rtf) and a parameter file (TYDN.prm) were used to generate and minimize the complex structure, respectively. These topology and parameter files are given in the Supporting Information (Sections S1 and S2). Figure S1 shows a 2-D representation of the covalently bound EctopoI residue and ssDNA nucleotide portions (Supporting Information, Section S1). To check usefulness of our approach in the MD simulation-based studies of other type of topoIccs, we also created the HtopoIcc and successfully minimized the covalent complex structure. Since the active site tyrosine, Y723, [26] in HtopoI forms a covalent linkage with 3’ DNA, unlike Y319 in EctopoI forms covalent complex with 5’ DNA, we needed to use a slightly different TYDN.rtf and TYDN.prm files for 3’ DNA as given in the Supporting Information (Sections S1 and S2).

Virtual screening (VS)

We performed VS of NCI DTP library SMs taking the minimized EctopoIcc structure as a target. We independently performed the screening of the same library of SMs against the minimized EctopoI conformation as well. Notably, EctopoI coordinates used as the target here was extracted from the same minimized EctopoIcc conformation. We selected 2263 soluble SMs from the library of 2642 total SMs. We examined docked position of SMs for being near our target area, the Y319 cleavage site, as described in virtual screening subsection of the Experimental section. We considered NSC76027, one of the top hit SMs based on affinity obtained from VS that lie near the active site, as a model SM just to demonstrate the usefulness of our approach in the new antibacterial drug development. This SM has also been identified as SerB2 (phosphoserine phosphatase) enzyme inhibitor.[27] Since we used minimized structures of EctopoIcc, we believe that this EctopoI reaction intermediate enhances the significance of the screening results. In support of this approach of employing the EctopoIcc, the loop and alpha helices near the NSC76027 binding site

show significant structural variation between the EctopoI-DNA covalent and non-covalent complex (PDB 1MW8[28]) with RMSD value of 4.0 Å (Figure S2, Supporting Information, Section S3). Our procedure should therefore facilitate structure-based antibacterial drug development targeting bacterial DNA topoisomerases. Our procedure is also applicable for other DNA topoisomerases, including HtopoI.

Surface plasmon resonance (SPR)

We used SPR experiments to validate the selective direct binding of NSC76027 to EctopoI, to examine whether NSC76027 shows concentration dependent binding to EctopoI, and to determine equilibrium dissociation constant (K_D) of the interaction. In the validation experiment, we injected NSC76027 solution at 5 μM concentration over the CM5 sensor surface. SPR sensorgrams demonstrating the selective binding of NSC76027, to EctopoI as shown in Figure 2A. At 5 μM, NSC76027 binds to EctopoI with a response amplitude much higher as compared to Ezrin, a control protein immobilized using identical surface chemistry as for EctopoI on the same CM5 chip surface. The negative control analyte, NSC14975, does not bind to the immobilized EctopoI. We then performed SPR-based dose response assays for NSC76027. In the dose response assays, we independently immobilized EctopoI and Ezrin on another CM5 chip in a similar fashion as in the selective binding tests. Both analytes (NSC76027 and NSC14975) were serially diluted in buffer solutions. SPR sensorgrams for NSC76027 binding to EctopoI in a concentration dependent manner are shown in Figure 2B. The two continuous lines with same color indicate the technical reproducibility of the SPR sensorgrams for the same concentrations recorded in duplicate. We repeated NSC76027 dose response at least three times with different concentration range of NSC76027. As expected, a control experiment with NSC14975 (negative control analyte) exhibited no binding to EctopoI as shown in Figure 2C.

We further conducted SPR assays to determine the K_D of NSC76027-EctopoI interaction. As shown in Figure 2D, in the single cycle approach, various concentrations of the same analyte (NSC76027) were injected one after another, in increasing concentrations in the same cycle of the run. The experimental SPR sensorgrams (green continuous lines) were fitted to 1:1 kinetics binding model (dashed lines) to extract the K_D of NSC76027-EctopoI binding and we obtained a K_D value of ~80 nM for the interaction. We also repeated kinetics experiments two more times with multicycle kinetics with different NSC76027 concentration ranges. As expected, we obtained very similar K_D values (79±8 nM, average ±s.d., from three experimental replicates) for the NSC76027-EctopoI interaction when experimental data were fitted to the same 1:1 kinetics model. As expected, there is no dose response for NSC76027 binding to Ezrin (blue continuous lines, Figure 2D) to determine K_D value by fitting. SPR experiments thus confirm selective direct binding of NSC76027 to EctopoI as predicted by *in silico* VS. Moreover, the NSC76027-EctopoI binding is concentration dependent with nanomolar affinity.

Relaxation inhibition assay

We carried out relaxation assays for inhibition of EctopoI relaxation activity in the presence of NSC76027. In vitro relaxation inhibition assay also showed that NSC76027 was able to inhibit the relaxation activity of EctopoI in a dose dependent manner (Figure 3A). As

displayed in Figure 3B, NSC76027 inhibited 50% of the enzyme activity at ~2.2 μM (IC_{50} value). A relaxation inhibition assay with the negative control SM showed that NSC14975 does not inhibit the EctopoI relaxation activity even at 125 μM with 25 μM NSC76027 was also used as the positive control, which completely inhibits the relaxation activity (Figure 3C). NSC76027 also inhibits the relaxation activity of *M. tuberculosis* topoI (MttopoI) with an IC_{50} value of ~3.0 μM (data not shown).

Molecular dynamics (MD) simulations

The dynamics of the ternary complex was investigated using MD simulations taking the optimized NSC76027 conformation (Supporting Information, Section S4). A movie of the MD simulation (Supporting Information, Section S5) shows the dynamics of the ternary complex. Notably, NSC76027 resides within the EctopoI-ssDNA binding interface, near the ssDNA cleavage site. As depicted by RMSD measurements (Figure 4A), the overall ternary complex structure was stable after ~40 ns of the simulation time. Figure 4B shows the radius of gyration (R_g) measurement of the ternary complex. The measurements of R_g further demonstrate the thermal stability of the ternary complex after ~40 ns of the simulation time. For comparison, we also performed the 100 ns CPT simulations for EctopoIcc only. The blue colored lines in Figures 4A and 4B correspond to measurements for EctopoIcc only for the same 100 ns simulation time as for the ternary complex.

We have also calculated the binding free energy for NSC76027 binding to EctopoIcc using simulation trajectories with MM/GBSA approach and obtained a favorable binding energy of −35.1±7.1 kcal/mol for the binding. Here the average±s.d. values are obtained from the binding free energy calculated for each frame. Figure 5 depicts the ternary complex, after 100 ns of MD simulations, zoomed within the EctopoI-ssDNA binding interface.

Our 100 ns of CPT simulation result shows that NSC76027 forms hydrogen bonds with EctopoI. There are three hydrogen bonds formed between NSC76027 and EctopoI residues (ARG369, HIS365, and GLU366) with more than 50% occupancy (Table S1, Supporting Information, Section S6) of the simulation frames. A representative 2-D interaction diagram for formation of these hydrogen bonds are shown in Figure 6. Figure S2 (Supporting Information, Section S6) shows such 2-D representations at 50 ns, 75 ns, and 100 ns of the simulation time. As shown in Figure 6, there is a hydrogen bond formation between NSC76027 and EctopoI (ARG161) but this bond was not as stable (less than 10% occupancy) as compared to other three hydrogen bonds mentioned above.

Cell-based Assays

We conducted microbiological assays to measure the antibacterial activity of NSC76027. We could not detect antibacterial activity against *E. coli* MG1655, likely because of difficulty in penetration of this Gram-negative bacterium, or efflux pump action. Previous genetic studies have shown that topoI is essential for the viability of mycobacteria and a validated target for the discovery of new anti-tubercular drugs. [9c, 29] We found that NSC76027 inhibits the growth of *M. smegmatis* (MIC=25 μM) and *M. tuberculosis* H37Rv (MIC=35 μM).

Discussion

DNA topoisomerases change the topological state of DNA, which is important for key cellular processes. Bacterial DNA topoisomerases are major target biomolecules for the discovery of new antibacterial drugs.[3] It has been shown that the accumulation of bacterial topoIcc leads to the bacterial cell death.[7a] The inhibition of type IIA bacterial topoisomerases as well as type IB HtopoI and type IIA human topoisomerase using poison inhibitors are very important in the discovery of antibacterial or anticancer therapeutics.[3] Herein, we are motivated to design a model and develop procedures to handle the covalent complex between bacterial DNA topoI and DNA for computation-based investigations using the CHARMM36 force field, which to the best of our knowledge, have not been conducted previously. For structure-based drug development targeting DNA topoisomerases using computational methods, it is crucial to investigate such a covalent complex. The action of small molecules acting as bacterial topoI poison inhibitors can potentially lead to discovery of new antibacterial drugs. MD simulations is helpful to visually confirm the stability of the topoI-SM-DNA ternary complex, which is essential for the inhibitor to be a poison inhibitor of bacterial topoisomerase as well as allows the investigation of target-inhibitor interactions for the stability of the bacterial topoI-SM-DNA ternary complex. As a model system, we have considered EctopoI, which is the most extensively studied bacterial topoI for the discovery of antibacterial drugs.

We have used TYDN.rtf and TYDN.prm files together with standard CHARMM36m force field to establish the covalent linkage between O^{S}_{319} and $C^{5'}_{9}$ (Figure 1), minimize the structure for target used in VS, and perform MD simulation of the ternary complex. These two topology and parameter files (TYDN.rtf and TYDN.prm, Supporting Information, Sections S1 and S2) are easy to use and the idea that we adopted to establish EctopoI covalent linkage with ssDNA (between O^{S}_{319} and $C^{5'}_{9}$) is very straightforward.

Since topoI forms a transient covalent linkage with a single DNA strand, the EctopoIcc target enhances the significance of screening results. Taking this into account, we minimized the EctopoIcc structure (Section 2.3) using TYDN.rtf and TYDN.prm files (Supporting Information, Sections S1 and S2). The minimized EctopoIcc was then used as the screening target. We then performed VS of NCI DTP library of SMs against this minimized EctopoIcc target. From the minimized structure, the protein coordinates were also used to generate PDBQT files for EctopoI only conformation and perform an independent screening of the same SMs against this EctopoI only target. Out of 2263 SMs, 2008 SMs successfully passed through screening resulting output files with affinity values. This discrepancy might be due to poor structural transformation (from 2-D to 3-D) of remaining SMs. We selected one of the top hit SMs, NSC76027, as a model SM for further investigations. We expect that NSC76027 will recognize EctopoI to inhibit the DNA relaxation. We have carried out a series of SPR experiments to demonstrate favorable binding of NSC76027 with EctopoI as well as relaxation inhibition assays to demonstrate the inhibition of EctopoI relaxation activity. These experimental results confirm on one hand that NSC76027 specifically binds to EctopoI and on the other hand it prevents the DNA relaxation activity of EctopoI with clear dose dependence. A scheme of both computational as well experimental procedures

that we followed to carry out our investigations is shown in the Supporting Information (Figure S4, Section S7). We could not detect specific interaction between NSC76027 and ssDNA fragments for our 100 ns CPT simulation time. The simulation time used here might not be long for enough structural rearrangements in EctopoIcc structure to allow the formation of hydrogen bonds between NSC76027 and ssDNA. It is also possible that NSC76027 binds to EctopoI to prevent the formation of the complex with DNA. Mechanistic and structural studies in future experiments will address this interaction mechanism.

The optimized NSC76027 confirmation was used to establish the ternary complex and the ternary complex was simulated for 100 ns under CPT conditions. The covalent linkage was stable for 100 ns of the simulation time. Biomolecular interfaces are the area where small molecules have binding preference, establishing interfacial interactions, due to imperfection of packing at the interface.[30] It has also been found that some interfacial residues, with higher probability of being pocket residues, have only a smaller fraction of their surface area accessible to solvent and are promising ligand binding sites.[31] Such interfacial interaction[32] may promote the trapping of EctopoIcc by forming a stable ternary complex. The accumulation of these ternary complexes in bacterial cell ultimately may lead to the bacterial cell killing.

There are many libraries of SMs available for virtual screening. In this report, we only intend to demonstrate the usefulness of our model for molecular simulations that handles bacterial topoIcc, which has importance in new antibacterial drug development. Besides, implementation of additional filters to the solubility filter may allow selection of the molecules with adequate permeability. Furthermore, there are different subfamilies of DNA topoisomerases that form covalent complexes with single or double strands of DNA. However, the formation of the covalent complexes all involve the covalent linkage of active site tyrosine with the DNA phosphate at the cleavage site that our model is capable of handling. We believe that our method and procedures described in this report may be utilized for the covalent complex of other DNA topoisomerases and single or double stranded DNA, including HtopoI that is one of the targets for anticancer drug development. We have generated HtopoIcc following our approach and preformed a short simulation for this structure using a slightly modified TYDN.rtf and TYDN.prm (Supporting Information, Sections 1 and 2) files together with CHARMM36m force field. The modification was needed to handle tyrosine-DNA covalent bond at 3’ DNA end. Indeed, our approach works for this system as well. Future investigations, including longer simulations, for HtopoIcc will be carried out. Our procedure is therefore an important step in computer aided structure-based drug development that requires investigations of both topoI-DNA covalent complex both in presence and absence of hit SMs. Based on results presented in this manuscript, several avenues will open for future mechanistic studies in expanding the current investigations or exploration of new drug candidates.

Conclusions

Trapping transient covalent complex of DNA topoI and DNA in bacterial cells using topoI poison inhibitors leads to accumulation of such complexes, which ultimately kills the

bacterial cells. Computational investigations, including MD simulations, of small molecules as bacterial topoI poison inhibitors requires handling of the covalent complex of bacterial topoI and DNA, which, to the best of our knowledge, has not been previously reported. Motivated by this, we designed the topoI-DNA covalent complex model and performed MD simulations to investigate the dynamics of the ternary complex. Our EctopoI-DNA covalent complex model is relatively simple and the procedures described here are straightforward to implement in other topoisomerase systems, including HtopoI.

Experimental Section

Wild type EctopoI-ssDNA structure set up:

PDB IDs 3PX7[10a] and 4RUL[10b] were used to model a full length EctopoIcc. Notably, 4RUL is a full length EctopoI in complex with ssDNA whereas 3PX7 is a shorter sequence of EctopoI covalently bound to ssDNA. Hence, to get the full length EctopoI in covalent complex with ssDNA, we structurally aligned the 4RUL structure over 3PX7 and saved the CTD from the aligned 4RUL. This aligned CTD was connected to 3PX7. Therefore, 4RUL is the template for the CTD. We also manually added missing DNA nucleotides in 3PX7 with the same nucleotides in 4RUL, using VMD. Missing residues were completed using MODELLER[33] with replacing the phosphotyrosine (PTR) engineered residue (residue ID 319) in 3PX7 by tyrosine and the mutated amino acid residue N111 in 3PX7 was also converted back to D111 using CHARMM-GUI[34] to have EctopoI in its wild-type form. The missing ssDNA nucleotides in 3PX7 were also added using VMD[35] The resulting structure has Zn2+ but no Hg2+ atoms. PDB ID 1K4T[26] was used to model and simulate the HtopoIcc.

Generation of EctopoI-DNA covalent complex (EctopoIcc):

The ssDNA nucleotides in the full length EctopoIcc, after adding the missing nucleotides in crystal structure 3PX7, are present as 5’AATGCGCT↓ TTGGG3’, where the arrow shows the ssDNA cleavage site. In this manuscript, the ssDNA nucleotides or atoms in these nucleotides will be identified as their position (from 5’ to 3’) along with their names. Using VMD[35] and CHARMM36m force field as well as the TP1 phosphotyrosine patch together with a topology file (TYDN.rtf, Supporting Information, Section S1), first Y319 was phosphorylated and then a linkage between phosphorylated Y319 in EctopoI and 5’ ssDNA end was established. The resulting structure and data files (.psf and .pdb files) now have EctopoI-ssDNA covalent linkage. Slightly modified TYDN.rtf (Supporting Information, Section S1) was used to generate the HtopoIcc.

Energy minimization:

EctopoIcc was solvated using VMD in a cubic box of dimension 140×140×140 Å3 with TIP3 water and then electrically neutralized with NaCl and NaCl concentration was set to 50 mM. The resulting system comprised of 261,332 atoms. The energy minimization was carried out for 10,000 steps using NAMD package[36] with parameters in CHARMM36m force field together with parameters in TYDN.prm (Supporting Information, Section S2), using the conjugate gradient and line search algorithm. We used the Particle Mesh Ewald (PME)[37] method for the long-range interactions with 12Å non-bonded cut-off. Slightly

modified TYDN.prm (Supporting Information, Section S2) was used to minimize the HtopoIcc.

Virtual screening (VS):

Open Babel[38] was used to generate ligand input files (PDBQT files). Briefly, two-dimensional structures of NCI DTP library SMs (Diversity Set V, Mechanistic Set IV, Approved Oncology Drugs Set VI, and Natural Products Set III) were converted to three-dimensional (3-D) structures and then to PDBQT file formats. We selected only 2263 soluble SMs from the entire set of SMs. These 3-D structures were minimized for 10,000 steps using obminimize and then random ligand conformer of each minimized SM was generated using obconformer in Open Babel followed by conversion to PDBQT files with addition of polar hydrogen atoms. The minimized EctopoIcc as well as EctopoI coordinates extracted from the same EctopoIcc were converted to PDBQT files using AutoDockTools[39] (version 1.5.6) with addition of polar hydrogen atoms to use as the screening targets. Finally, AutoDock Vina[40] (version 1.1.2) was used in VS of ligands against the targets. The screening was performed using a search box with dimensions 118×80×84 Å3, which covered the entire EctopoIcc or EctopoI. The docked positions of top ranked SMs for EctopoIcc with affinity greater than −10 kcal/mol were examined for being near our target area, the Y319 cleavage site. We also examined the docked position of the selected SMs to determine whether they are docked nearby the Y319 site in the EctopoI only target with equal or no less than 90% affinities as compared to the docked affinities with EctopoIcc. The selected SMs with higher affinity values were first ranked based on affinity for EctopoIcc and then ranked again based on affinity for EctopoI only.

Surface plasmon resonance (SPR):

Biacore T200 SPR instrument (GE Healthcare) was used to carry out the SPR experiments. EctopoI was immobilized as a ligand on a CM5 chip (GE Healthcare) to a level of ~20,000 Response Units (RU) in the presence of 10 mM sodium acetate buffer at pH 5.5. Ezrin was also immobilized as a control ligand. A standard amine coupling chemistry according to the manufacturer's recommended protocol (GE Healthcare) was used to capture ligands. PBS-P + (0.2 M phosphate buffer, pH 7.4, 27 mM KCl, 1.37 M NaCl, and 0.5% v/v surfactant P20) buffer was diluted 10X in ddH2O and filtered through a 0.22 μM polystyrene membrane filter (referred to as PBS-P hereafter) and then used as the immobilization running buffer. NSC76027, one of the hit SMs used as analyte, was injected over the ligand immobilized CM5 chip surfaces in various concentrations in the presence of the PBS-P buffer and supplemented with 1% v/v DMSO and filtered through a 0.22 μM polystyrene membrane (referred to as PBSP+1%DMSO hereafter). The same PBS-P+1% DMSO buffer was used as the running buffer in the analyte-ligand binding experiments. NSC14975 was also used as a negative control analyte. A 1:1000 (v/v) H_3PO_4 solution (H_3PO_4:ddH_2O) or 2 M NaCl was used to regenerate the CM5 chip sensor surface (injected for 20 s). A flow rate of 30 μL/min or 50 μL/min was maintained during analyte injections and the regeneration solutions. One flow cell (FC) was used for reference (RFC) and another FC next to the RFC of the same CM5 chip was used as an active FC (AcFC). Analyte solutions were injected on both FCs in duplicate for each concentration. The RFC has the same surface chemistry as the AcFC but immobilized ligands (EctopoI or Ezrin). SPR sensorgrams for PBS-P+1% only injections

were also recorded for blank subtraction. The sensorgrams obtained for analysis were both reference (signals from RFC) and blank (signals for PBS-P+1% DMSO only) subtracted.

Relaxation inhibition assay:

Recombinant EctopoI, expressed in *E. coli*, was purified as described previously.[41] EctopoI relaxation activity inhibition by NSC76027 was assayed in a buffer containing 10 mM Tris-HCl, pH 8.0, 50 mM NaCl, 0.1 mg/ml gelatin, and 0.5 mM MgCl2. Half a microliter of NSC76027 dissolved in DMSO or solvent alone was mixed with 10 μl of the reaction buffer containing 10 ng of enzyme before the addition of 9.5 μl of reaction buffer containing 160 ng of supercoiled pBAD/Thio plasmid DNA purified by cesium chloride gradient as the substrate. Following incubation of the mixtures at 37°C for 30 min, the reactions were terminated by the addition of 4 μl of 50% glycerol, 50 mM EDTA, and 0.5% (v/v) bromophenol blue and the mixtures were analyzed by agarose gel electrophoresis. The gels were stained in ethidium bromide and photographed under UV light.

Molecular dynamics (MD) simulations:

LigParGen webserver[42] was used to generate topology and parameter files of the NSC76027 optimized structure (NSC76027 input files). All-atom MD simulations were performed using the NAMD simulation package[36] for EctopoIcc alone and the ternary complex. The input files (.psf and .pdb files) for MD simulations were generated by using VMD [37] with CHARMM36m force field together with TYDN.rtf (Supporting Information, Section S1) and the NSC76027 input files. The EctopoIcc and ternary complex structures were solvated using VMD[35] in a cubic box of dimension 140×140×140 Å3 with TIP3 water and then electrically neutralized by adding NaCl and NaCl concentration was set to 50 mM. The resulting EctopoIcc and ternary complex system comprised of 261,332 and 261,150 atoms, respectively. This ternary complex structure has the EctopoI-ssDNA covalent linkage generated using the same procedures as mentioned in the Experimental section, with no covalent bonding of NSC76027 with EctopoI and ssDNA. The EctopoIcc and ternary complex systems were minimized for 10,000 steps. CHARMM36m force field parameter files, TYDN.prm file (Supporting Information, Section S2), and parameter file from the NSC76027 input files were used to minimize the complex structures. The minimized complex structures were then equilibrated at 300 K (27 °C) for 100 ps with protein heavy atoms harmonically restrained at a 1 fs integration time step. Finally, the simulations were propagated with Langevin dynamics with a damping constant of 1 ps^{-1} for 100 ns under CPT condition with a time step of 2 fs for 100 ns. MD simulations for HtopoIcc were carried out using a slightly modified TYDN.prm file, for 3’ DNA end, together with the same CHARMM36 force field parameter files as mentioned above.

Cell-based Assays:

M. smegmatis mc2155 cells were grown first at 37 °C in 7H9 media supplemented with 0.2% glycerol, 0.05% Tween 80, and 10% albumin, dextrose, sodium chloride (ADN) to saturation and then diluted 1:50 in 7H9 without ADN. After growing overnight to saturation again, cells adjusted to OD_{600} =0.1 were diluted 1:5 in 7H9 media. Aliquots of 50 μL of the diluted cells corresponding to ~106 cells were then added to a clear-bottom 96-well plate that contained 50 μL of the serially diluted compound in 7H9 media. Resazurin was

added[43] in a final concentration of 0.02% to all the wells of the plate after 48 hours of incubation, and fluorescence readings at λ_{ex} 528/20 and λ_{em} 590/35 were obtained to determine the Minimum Inhibitory Concentration (MIC) values. The MIC was recorded as the concentration that prevented at least 90% growth when compared to the control wells with DMSO. Antibacterial activity against *E. coli* MG1655 was assayed in Müller–Hinton broth (MHB). MIC against *M. tuberculosis* were determined by a modified microplate Alamar blue assay (MABA) as a service provided by the Institute for Tuberculosis Research at University of Illinois at Chicago.

Data Analysis:

Images of agarose gels from the relaxation inhibition assay were analyzed using AlphaView software (San Jose, CA) to quantitate the supercoiled DNA bands. Inhibition was calculated as the percentages of supercoiled DNA that was not relaxed in the presence of different concentrations of NSC76027. The non-linear fitting of in vitro relaxation inhibition data using four-parameter variable slope model was accomplished by GaphPad prism (La Jolla, CA). Biacore T200 evaluation software version 1.0 (GE Healthcare) was used to visualize the SPR sensorgrams and generate data for plotting. VMD[35] was used to analyze simulation trajectories, to determine radius of gyration of NSC76027, to measure RMSD values, and to visualize as well as generate pictures of structures. Calculation of binding free energy using MM/GBSA approach was performed using NAMD. Each frame in the NVT simulation trajectory file was saved at every 200 ps. Carma[44] was used to determine massweighted radius of gyration (Rg) of the simulation trajectories. An atomic distance of 3.5Å and angle cut off of 30 degrees were used to trace hydrogen bonding, using VMD.[35] 2-D ligand interaction maps were generated using Schrödinger Maestro.[45] GaphPad prism was used to draw graphs.

Supplementary Material

Refer to Web version on PubMed Central for supplementary material.

Acknowledgements

The experimental SPR sensorgrams were measured using a Biacore T200 instrument and were evaluated using the Biacore T200 evaluation software version 1.0 available in the Biacore Molecular Interaction Shared Resource (BMISR) facility at Georgetown University. The BMISR is supported by NIH grant P30CA51008. This work was also supported by NIH grant R01GM054226 (YT).

References:

[1]. a)Champoux JJ, Annu Rev Biochem 2001, 70, 369–413; [PubMed: 11395412] b)Corbett KD, Berger JM, Annu. Rev. Biophys. Biomol. struct 2004, 33, 95–118; [PubMed: 15139806] c)Wang JC, Nat. Rev. Mol. Cell Biol 2002, 3(6), 430–440. [PubMed: 12042765]

[2]. Tse YC, Kirkegaard K, Wang JC, J. Biol. Chem 1980, 255(12), 5560–5565. [PubMed: 6155377]

[3]. Pommier Y, ACS Chem. Biol 2013, 8(1), 82–95. [PubMed: 23259582]

[4]. Delgado JL, Hsieh C-M, Chan N-L, Hiasa H, Biochem. J 2018, 475(2), 373–398. [PubMed: 29363591]

[5]. Sadaie MR, Mayner R, Doniger J, Antiviral Res. 2004, 61(1), 1–18. [PubMed: 14670589]

[6]. Anderson VE, Osheroff N, Curr. Pharm. Des 2001, 7(5), 337–353. [PubMed: 11254893]

[7]. a)Tse-Dinh YC, Nucleic Acids Res. 2009, 37(3), 731–737; [PubMed: 19042977] b)Cheng B, Shukla S, Vasunilashorn S, Mukhopadhyay S, Tse-Dinh YC, J. Biol. Chem 2005, 280(46), 38489–38495. [PubMed: 16159875]

[8]. Usongo V, Drolet M, PLOS Genet. 2014, 10(8), e1004543. [PubMed: 25102178]

[9]. a)Tse-Dinh Y-C, Future Med. Chem 2015, 7(4), 459–471; [PubMed: 25875873] b)Sandhaus S, Chapagain PP, Tse-Dinh Y-C, Sci. Rep 2018, 8(1), 1437; [PubMed: 29362471] c)Nagaraja V, Godbole AA, Henderson SR, Maxwell A, Drug Discov. Today 2017, 22(3), 510–518. [PubMed: 27856347]

[10]. a)Zhang Z, Cheng B, Tse-Dinh Y-C, Proc. Natl. Acad. Sci 2011, 108(17), 6939–6944; [PubMed: 21482796] b)Tan K, Zhou Q, Cheng B, Zhang Z, Joachimiak A, Tse-Dinh Y-C, Nucleic Acids Res. 2015, 43(22), 11031–11046. [PubMed: 26490962]

[11]. Lynn RM, Wang JC, Proteins: Struct., Funct. Bioinf 1989, 6(3), 231–239.

[12]. Drlica K, Trends Genet. 1990, 6, 433–437. [PubMed: 1965069]

[13]. Kitchen DB, Decornez H, Furr JR, Bajorath J, Nat. Rev. Drug Discov 2004, 3(11), 935–949. [PubMed: 15520816]

[14]. Oviatt AA, Kuriappan JA, Minniti E, Vann KR, Onuorah P, Minarini A, De Vivo M, Osheroff N, Bioorg. Med.Chem. Lett 2018, 28(17), 2961–2968. [PubMed: 30006062]

[15]. a)Meng XY, Zhang HX, Mezei M, Cui M, Curr. Comput. Aid Drug Discov 2011, 7(2), 146–157;b)Dreger A, Kharwb O, Agoglitta O, Bülbül EF, Melesina J, Sippl W, Holl R, ChemMedChem 2019, 14(8), 871–886. [PubMed: 30801965]

[16]. a)Lionta E, Spyrou G, Vassilatis DK, Cournia Z, Curr. Top. Med. Chem 2014, 14(16), 1923–1938; [PubMed: 25262799] b)Medarametla P, Gatta V, Kajander T, Laitinen T, Tammela P, Poso A, ChemMedChem 2018, 13(22), 2400–2407. [PubMed: 30178912]

[17]. a)Durrant JD, McCammon JA, BMC Biol. 2011, 9(1), 71; [PubMed: 22035460] b)Ghattas MA, Bryce RA, Al Rawashdah S, Atatreh N, Zalloum WA, ChemMedChem 2018, 13(6), 500–506. [PubMed: 29058775]

[18]. Sakano T, Mahamood MI, Yamashita T, Fujitani H, Biophys. Physicobiol 2016, 13, 181–194. [PubMed: 27924273]

[19]. Klebe G, Drug Discov. Today 2006, 11(13), 580–594. [PubMed: 16793526]

[20]. Lavecchia A, Di Giovanni C, Curr. Med. Chem 2013, 20(23), 2839–2860. [PubMed: 23651302]

[21]. Nepal P, Saldin DK, Phys. Rev. B 2018, 97(19), 195426.

[22]. a)Tiwari PB, Chapagain PP, Üren A, Sci. Rep 2018, 8(1), 10557; [PubMed: 30002427] b)Tiwari PB, Chapagain PP, Banda S, Darici Y, Üren A, Tse-Dinh Y-C, FEBS Lett. 2016, 590(17), 2844–2851. [PubMed: 27448274]

[23]. Perilla JR, Hadden JA, Goh BC, Mayne CG, Schulten K, J. Phys. Chem. Lett 2016, 7(10), 1836–1844. [PubMed: 27128262]

[24]. a)Palermo G, Minniti E, Greco ML, Riccardi L, Simoni E, Convertino M, Marchetti C, Rosini M, Sissi C, Minarini A, De Vivo M, Chem. Commun 2015, 51(76), 14310–14313;b)Jiang Z, Zhang Z, Cui G, Sun Z, Song G, Liu Y, Zhong G, Front. Chem 2018, 6(456);c)Sari L, Andricioaei I, Nucleic Acids Res. 2005, 33(20), 6621–6634; [PubMed: 16314322] d)D'Annessa I, Coletta A, Sutthibutpong T, Mitchell J, Chillemi G, Harris S, Desideri A, Nucleic Acids Res. 2014, 42(14), 9304–9312; [PubMed: 25056319] e)Huang N-L, Lin J-H, Nucleic Acids Res. 2015, 43(14), 6772–6786; [PubMed: 26150421] f)Chen S-F, Huang N-L, Lin J-H, Wu C-C, Wang Y-R, Yu Y-J, Gilson MK, Chan N-L, Nat. Commun 2018, 9(1), 3085. [PubMed: 30082834]

[25]. Cinelli MA, Med. Res. Rev 2019, 39(4), 1294–1337. [PubMed: 30456874]

[26]. Staker BL, Hjerrild K, Feese MD, Behnke CA, Burgin AB, Stewart L, Proc. Natl. Acad. Sci 2002, 99(24), 15387–15392. [PubMed: 12426403]

[27]. Arora G, Tiwari P, Mandal RS, Gupta A, Sharma D, Saha S, Singh R, J. Biol. Chem 2014, 289(36), 25149–25165. [PubMed: 25037224]

[28]. Perry K, Mondragón A, Structure 2003, 11(11), 1349–1358. [PubMed: 14604525]

[29]. a)Ravishankar S, Ambady A, Awasthy D, Mudugal NV, Menasinakai S, Jatheendranath S, Guptha S, Sharma S, Balakrishnan G, Nandishaiah R, Ramachandran V, Eyermann CJ, Reck F, Rudrapatna S, Sambandamurthy VK, Sharma UK, Tuberculosis 2015, 95(5), 589–598; [PubMed:

26073894] b)Ahmed W, Menon S, Godbole AA, Karthik PVDNB, Nagaraja V, FEMS Microbiol. Lett 2014, 353(2), 116–123. [PubMed: 24593153]

[30]. Gao M, Skolnick J, Proc. Natil. Acad. Sci 2012, 109(10), 3784–3789.

[31]. Walter P, Metzger J, Thiel C, Helms V, PLoS One 2013, 8(3), e58583. [PubMed: 23505538]

[32]. Pommier Y, Kiselev E, Marchand C, Bioorg. Med. Chem. Lett 2015, 25(18), 3961–3965. [PubMed: 26235949]

[33]. Eramian D, Shen M.-y., Devos D, Melo F, Sali A, Marti-Renom MA, Protein Sci. 2006, 15(7), 1653–1666. [PubMed: 16751606]

[34]. Lee J, Cheng X, Swails JM, Yeom MS, Eastman PK, Lemkul JA, Wei S, Buckner J, Jeong JC, Qi Y, Jo S, Pande VS, Case DA, Brooks CL, MacKerell AD, Klauda JB, Im W, J. Chem. Theory. Comput 2016, 12(1), 405–413. [PubMed: 26631602]

[35]. Humphrey W, Dalke A, Schulten K, J. Mol. Grap 1996, 14(1), 33–38.

[36]. Phillips JC, Braun R, Wang W, Gumbart J, Tajkhorshid E, Villa E, Chipot C, Skeel RD, Kalé L, Schulten K, J. Comput. Chem 2005, 26(16), 1781–1802. [PubMed: 16222654]

[37]. Darden T, York D, Pedersen L, J. Chem. Phys 1993, 98(12), 10089–10092.

[38]. O'Boyle NM, Banck M, James CA, Morley C, Vandermeersch T, Hutchison GR, J. Cheminf 2011, 3(1), 33.

[39]. Morris GM, Huey R, Lindstrom W, Sanner MF, Belew RK, Goodsell DS, Olson AJ, J. Comput. Chem 2009, 30(16), 2785–2791. [PubMed: 19399780]

[40]. Trott O, Olson AJ, J. Comput. Chem 2010, 31(2), 455–461. [PubMed: 19499576]

[41]. Narula G, Annamalai T, Aedo S, Cheng B, Sorokin E, Wong A, Tse-Dinh Y-C, J. Biol. Chem 2011, 286(21), 18673–18680. [PubMed: 21478161]

[42]. Dodda LS, Cabeza de Vaca I, Tirado-Rives J, Jorgensen WL, Nucleic Acids Res. 2017, 45(W1), W331–W336. [PubMed: 28444340]

[43]. Sarker SD, Nahar L, Kumarasamy Y, Methods 2007, 42(4), 321–324. [PubMed: 17560319]

[44]. Glykos NM, J. Comput. Chem 2006, 27(14), 1765–1768. [PubMed: 16917862]

[45]. Schrödinger Release 2019–4: Maestro, Schrödinger, LLC, New York, NY, 2019.

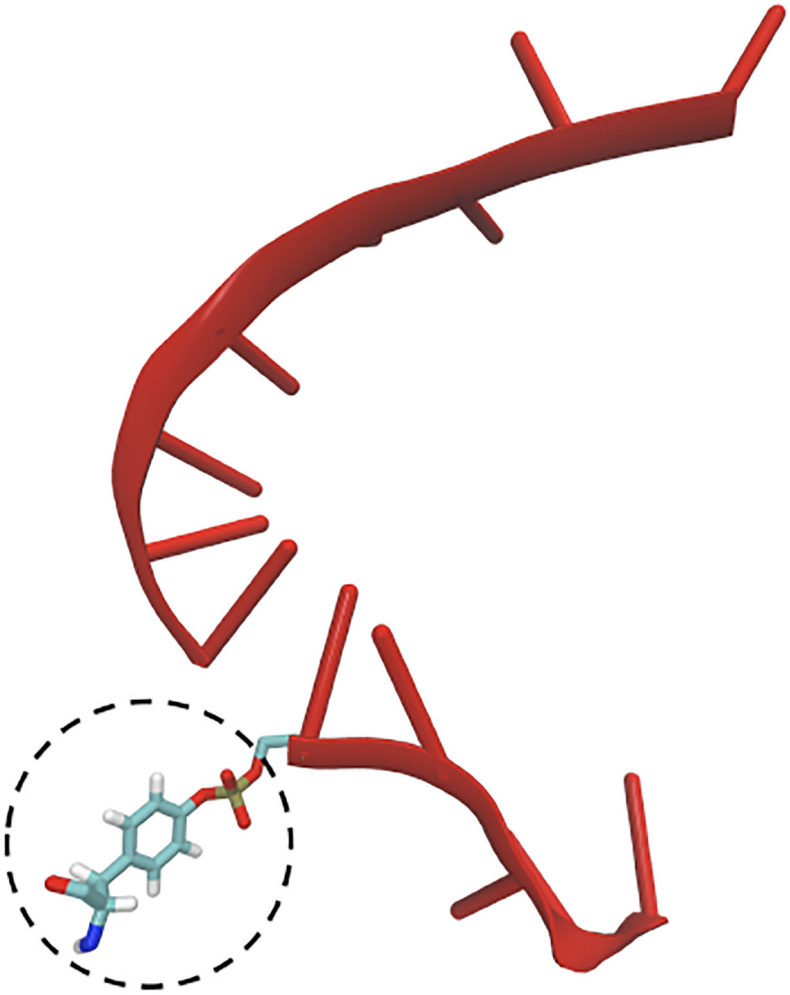

Figure 1.

Covalent linkage between EctopoI and ssDNA generated using our procedure. The nucleophile, Y319 of EctopoI upon phosphorylation, is represented within a dotted circle. One of the side chain oxygen atoms of the phosphorylated Y319 (O^{S}_{319}) is linked with 5' carbon of thymine in the 9th position ($C^{5'}_{9}$) of the ssDNA via a covalent bond.

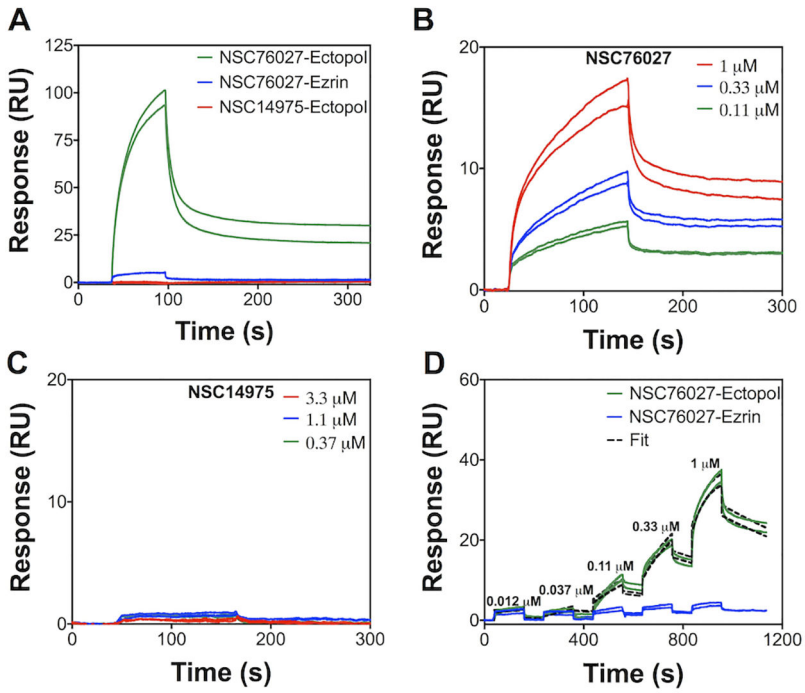

Figure 2.

A) SPR sensorgrams obtained in the selective binding test for NSC76027. SPR sensorgrams from dose response assays for: B) NSC76027 and C) NSC14975 binding to EctopoI. D) NSC76027 binding to EctopoI and Ezrin at different NSC76027 concentrations. The two continuous lines with the same color correspond to the SPR sensorgrams for the same concentrations recorded in duplicate for technical reproducibility and the dashed lines indicate fitting of experimental sensorgrams to a 1:1 kinetics binding model.

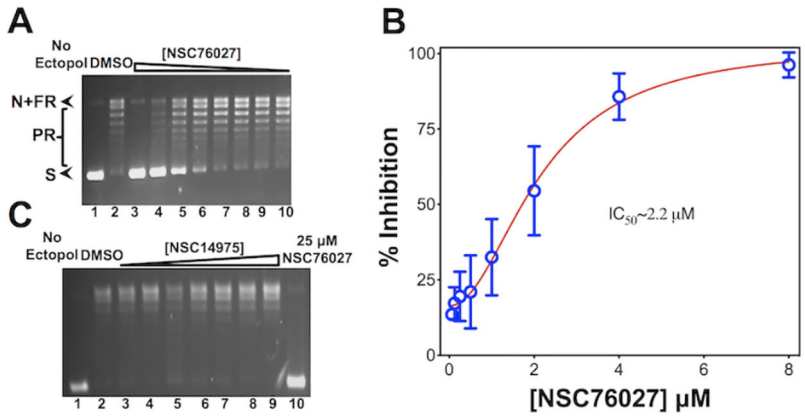

Figure 3.

A) Inhibition of EctopoI relaxation activity by NSC76027. Serial two-fold dilutions of NSC76027, starting with 8 µM in lane 3 and ending with 62.5 nM in lane 10. Lanes 1, control reaction mixture with no enzyme added; lanes 2, DMSO control. S: Supercoiled DNA, N: Nicked DNA, FR: Fully Relaxed DNA, PR: Partially relaxed DNA. C) IC_{50} of NSC76027. Symbols are the average percentage inhibition values from four different experiments with standard deviations shown as error bars. The red continuous line is the four-parameter variable slope non-linear fit to determine IC50 value, which is ~2.2 µM. C) Serial two-fold dilutions of NSC14975 (negative control analyte), starting with 125 µM in lane 9 and ending with 1.95 µM in lane 3. Lane 1: control reaction mixture with no enzyme added, lane 2: DMSO control, lane 10: 25 µM NSC76027.

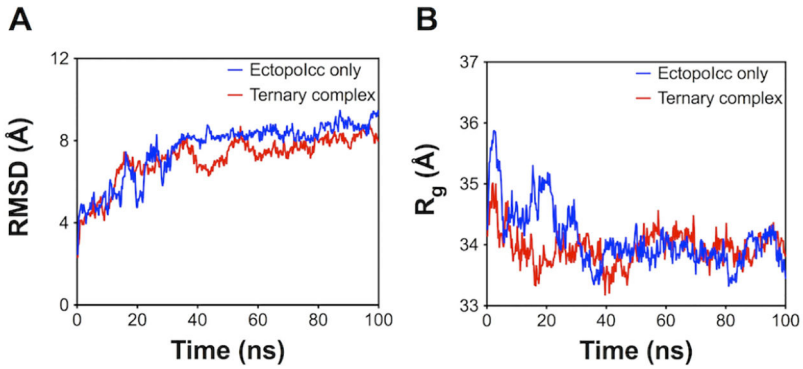

Figure 4.

A) RMSD measurements and B) Radius of gyration (R_g) of the ternary complex (EctopoI-NSC76027-ssDNA) structures obtained over the time course of MD simulations. The RMSD and Rg measurements for EctopoIcc are also shown for comparison.

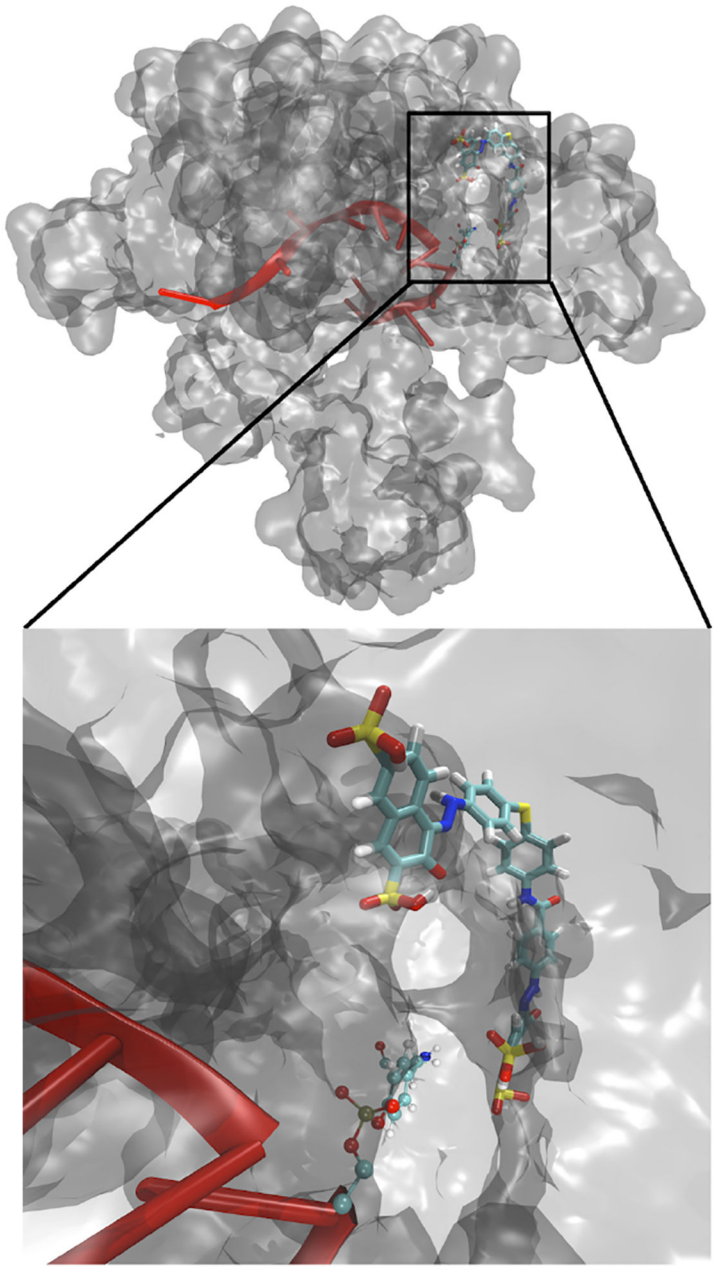

Figure 5.

The ternary complex after 100 ns of MD simulations zoomed near the ssDNA cleavage site. Grey colored structure represents EctopoI with colored CPK structure as Y319 in covalent complex with ssDNA, red colored structure represents ssDNA, and colored licorice structure represents NSC76027.

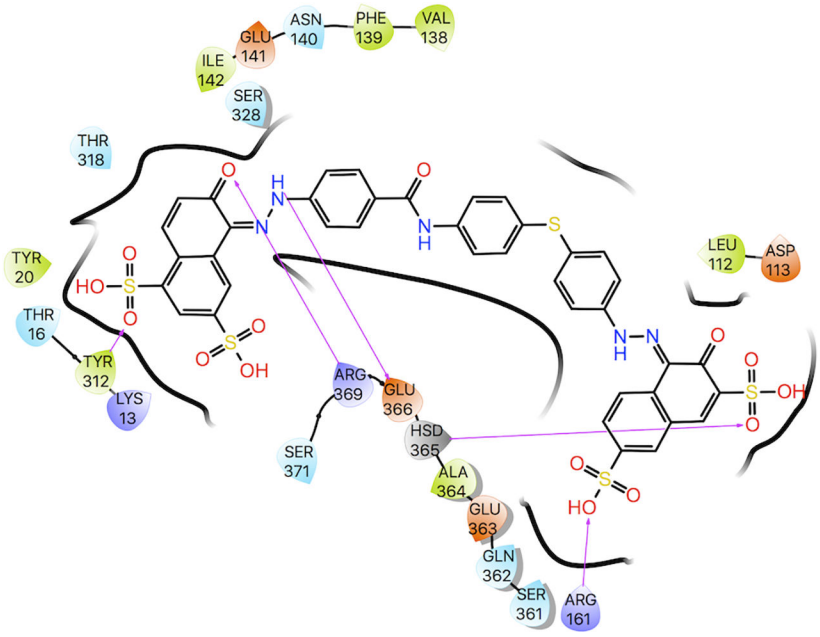

Figure 6.

Representative 2-D interaction diagram showing formation of hydrogen bonds between NSC76027 and EctopoI at 25 ns. The arrows that connect NSC76027 atoms with EctopoI residues represent the hydrogen bonds.